Vibrational and elastic properties of ferromagnesite across the electronic spin-pairing transition of iron

JUNG-FU LIN,[1,*] JIN LIU,[1] CALEB JACOBS,[1] AND VITALI B. PRAKAPENKA[2]

[1]Department of Geological Sciences, Jackson School of Geosciences, The University of Texas at Austin, Austin, Texas 78712, U.S.A.
[2]Center for Advanced Radiation Sources, The University of Chicago, Chicago, Illinois 60637, U.S.A.

ABSTRACT

Ferromagnesite $[(Mg,Fe)CO_3]$ has been proposed as a candidate host mineral for carbon in the Earth's mantle. Studying its physical and chemical properties at relevant pressures and temperatures helps our understanding of deep-carbon storage in the planet's interior and on its surface. Here we have studied high-pressure vibrational and elastic properties of magnesian siderite $[(Mg_{0.35}Fe_{0.65})CO_3]$ across the electronic spin transition by Raman and X-ray diffraction spectroscopies in a diamond-anvil cell. Our results show an increase in Raman shift of the observed lattice modes of magnesian siderite across the spin transition at 45 GPa as a result of an ~8% unit-cell volume collapse and a 10% stiffer lattice (higher bulk modulus). C-O bond lengthening in the strong, rigid $(CO_3)^{2-}$ unit across the spin transition contributes to a competitive decrease in Raman shift, most evident in the Raman shift decrease of the symmetric stretching mode. Combined vibrational and elastic results are used to derive the mode Grüneisen parameter of each mode, which drops significantly across the transition. These results suggest that the low-spin state has distinctive vibrational and elastic properties compared to the high-spin state. Analyses of all recent experimental results on the $(Mg,Fe)CO_3$ system show no appreciable compositional effect on the transition pressure, indicating weak iron-iron exchange interactions. Our results provide new insight into understanding the effects of the spin transition on the vibrational, elastic, and thermodynamic properties of $(Mg,Fe)CO_3$ as a candidate carbon-host in the deep mantle.

Keywords: Ferromagnesite, spin transition, X-ray diffraction, Raman spectroscopy, diamond-anvil cell

INTRODUCTION

Carbonates are the main form of carbon-bearing minerals on the Earth's surface and can be transported deep into Earth's mantle through subduction of oceanic lithosphere (Javoy 1997; Seto et al. 2008). Owing to the extremely low solubility of carbon in mantle silicates (Shcheka et al. 2006), carbon from plate subduction and primordial origins may exist primarily in accessory carbon compounds in the deep mantle. With increasing depth in the Earth's interior, these potential accessory deep-carbon hosts can exist in various forms such as CO_2 and hydrocarbon-rich fluids/melts, carbonates (calcite, dolomite, magnesite), diamond and graphitic compounds, and iron carbides, among others (e.g., Li and Fei 2003; Dasgupta and Hirschmann 2010; Kaminsky and Wirth 2011). Several studies have suggested that magnesite $(MgCO_3)$ could become the main host for carbon at the expense of calcite and dolomite at mantle conditions (Katsura and Ito 1990; Isshiki et al. 2004; Litasov et al. 2008). Although the redox state, amount of carbon, and potential existence of metallic iron in the deep Earth can all affect the stability of accessory carbon phases (Dasgupta and Hirschmann 2010), the observations of some carbonate inclusions in diamonds from the lower mantle have further supported magnesite as a major host of deep mantle carbon (Pal'yanov et al. 1999; Stachel et al. 2000; Brenker et al.

2007). Considering the average Fe/Mg molar ratio of ~0.12 in the Earth's mantle (McDonough and Sun 1995), the composition of carbonates in the mantle is likely to lie between magnesite $(MgCO_3)$ and siderite $(FeCO_3)$; these two end-member phases are known to form a continuous, solid solution, $(Mg,Fe)CO_3$. However, previous studies have shown that iron partitions strongly into coexisting silicates rather than into magnesite at relevant mantle pressure-temperature conditions (Ghosh et al. 2009; Stagno and Frost 2010; Rohrbach and Schmidt 2011). Nevertheless, studying the properties of Fe-bearing magnesite helps to elucidate deep-carbon storage in the mantle. Hereafter, the solid-solution component in the $MgCO_3$-$FeCO_3$ series is correctly referred to as ferromagnesite for the Mg-rich portion, or magnesian siderite for the Fe-rich portion of $(Mg,Fe)CO_3$, instead of plainly "siderite."

Recent experimental and theoretical studies have shown that magnesite remains chemically stable at the high pressure-temperature $(P$-$T)$ conditions of the deep mantle, even though a number of structural transitions in $MgCO_3$ have been reported (Biellmann et al. 1993; Isshiki et al. 2004; Oganov et al. 2008). The P-T conditions required to cause chemical dissociation and decarbonation of magnesite far exceed those present in the deep mantle, thus providing a possible storage mechanism for carbon in the lower mantle (Biellmann et al. 1993; Isshiki et al. 2004). An electronic high-spin (HS) to low-spin (LS) transition of Fe^{2+} is reported to occur in ferromagnesite at ambient temperature and ~40–45 GPa

* E-mail: afu@jsg.utexas.edu

by high-pressure X-ray emission and X-ray diffraction studies, as well as theoretical calculations (Mattila et al. 2007; Shi et al. 2008; Lavina et al. 2009, 2010a, 2010b; Nagai et al. 2010). The spin transition causes a volume collapse of ~6–10% and color changes (Lavina et al. 2009, 2010a, 2010b; Nagai et al. 2010). The low-spin ferromagnesite exhibits a smaller unit-cell volume than magnesite at corresponding pressures, suggesting that iron-rich magnesite may become more stable than magnesite at high P-T. However, although ferromagnesite is known to be stable up to at least 47 GPa and 2000 K (Santillan and Williams 2004) and up to 90 GPa at ambient temperature (Lavina et al. 2010a), it has been recently proposed that ferromagnesite transforms into an assemblage of a new high-pressure phase with three-membered rings of corner-sharing $(CO_4)^{4-}$ tetrahedra, together with magnesite and nano-diamonds (Oganov et al. 2008; Boulard et al. 2011). Furthermore, magnesite has been reported to undergo a structural phase transition at relevant P-T conditions of the lowermost mantle (Isshiki et al. 2004; Oganov et al. 2008).

Thus far, ferromagnesite is the only common deep-mantle carbonate mineral containing iron known to undergo the spin-pairing transition. Therefore, strong interest lies in the effects of the spin transition on the behavior of this deep mantle carbonate, with respect to its thermodynamic, elastic, and vibrational properties. Of particular interest are the effects of the spin transition of iron in ferropericlase [(Mg,Fe)O], the second most abundant mineral in the lower mantle, at 40–60 GPa and room temperature [see Lin and Tsuchiya (2008) for a recent review]. The known effects of the transition on the properties of ferropericlase, such as elasticity, electrical, and thermal conductivity, and deformation, have dramatically affected our understanding of the seismic, geochemical, and geomagnetic observations of the lower mantle (e.g., Lin et al. 2005, 2007; Speziale et al. 2005, 2007; Fei et al. 2007a; Crowhurst et al. 2008; Marquardt et al. 2009; Lin et al. 2009; Komabayashi et al. 2010). Experimental studies on the effects of the spin transition on the properties of ferromagnesite can thus provide more insight into understanding the effects of the spin transition in the lower-mantle ferropericlase. However, experiments need to be conducted on ferromagnesite with respect to the transition effects on the vibrational, elastic, and thermodynamic properties (Gillet et al. 1993; Zhang et al. 1998; Lavina et al. 2009, 2010a, 2010b; Nagai et al. 2010).

Here we have studied high-pressure Raman and X-ray diffraction spectra of magnesian siderite $(Mg_{0.35}Fe_{0.65})CO_3$ across the spin transition in a diamond-anvil cell (DAC). The high iron content in the sample allows us to see the effects of the spin transition on the vibrational and elastic parameters more clearly, although ferromagnesite is likely to contain a much smaller amount of iron at relevant P-T conditions of the deep mantle (Ghosh et al. 2009; Stagno and Frost 2010; Rohrbach and Schmidt 2011). We observed significant changes in vibrational Raman bands across the transition, whereas combined Raman and X-ray diffraction results allowed for the evaluation of the Grüneisen parameter for the high-spin and low-spin states. By studying the vibrational and elastic properties of magnesian siderite at high pressures, as well as the effect of composition on the spin transition in iron, we aim to provide new insight into the vibrational, elastic, and thermodynamic behavior of the candidate carbonate in the deep mantle.

EXPERIMENTAL METHODS

A natural magnesian siderite sample was obtained from the Vargas Gem and Mineral Collection of the Jackson School of Geosciences at the University of Texas at Austin (collection number: V3817). Based on electron microprobe analyses, the sample has a composition of $(Mg_{0.33}Fe_{0.65}Mn_{0.02})CO_3$, together with less than 1% of minor calcium impurity. For simplicity on the following discussion of the spin transition of iron, the composition is mostly presented as $(Mg_{0.35}Fe_{0.65})CO_3$, with the minor Mn content counted toward the total Mg content. The sample is a light yellowish-brown mineral in plain light that exhibits a rhombohedral habit with perfect {101} cleavage. Both single-crystal and powder X-ray diffraction analyses confirmed the calcite crystal structure (space group: $R\overline{3}c$) with lattice parameters, $a = 4.6742$ (±0.0010) Å and $c = 15.2788$ (±0.0050) Å, under ambient conditions. In this structure, $(CO_3)^{2-}$ anions are located at corners of the distorted octahedron with Fe^{2+} or Mg^{2+} cations, which form a unit cell that is essentially a distorted halite (or ferropericlase) cell along [111] direction (Wells 1984).

For Raman spectroscopic experiments, a piece of the single crystal with a thickness of 20 μm and a diameter of ~45–50 μm was cleaved off along the (101) rhombohedral plane of the original specimen and used as the starting sample. A rhenium gasket was pre-indented by a pair of diamond anvils having 200 μm flat culets to a thickness of 25 μm. A hole of 90 μm in diameter was drilled in the pre-indented gasket and used as a sample chamber. The starting sample was loaded into the sample chamber of a DAC with the (101) crystal plane faced toward the culet, together with a few ruby spheres as the pressure calibrant (Mao et al. 1978). Neon was loaded into the sample chamber as the pressure medium (Fei et al. 2007b) using a newly built high-pressure gas loader in the Mineral Physics Laboratory of the University of Texas at Austin. Before the Ne loading, the gas loading system was evacuated for 30 min to prevent any air and moisture contamination on the sample. The Raman system in the Mineral Physics Laboratory used for the experiments is equipped with a Coherent Verdi V2 laser with a 532 nm wavelength, an electron multiplying charge-coupled device (EMCCD), and a Shamrock spectrometer from Andor Technology. The laser power was limited to ~50 mW to avoid overheating of the sample. Each Raman spectrum was collected with an exposure time of ~15 min to ensure quality data analyses. Pressure uncertainties were calculated from multiple measurements from the ruby spheres before and after each spectrum were taken.

For X-ray diffraction experiments, the sample was ground to micro-sized powder, which was then slightly pressed to form a disk; caution was taken not to grind the sample too hard as we had noticed that the sample may become partially amorphous if extreme grinding was applied. A small powder disk with a thickness of 18 μm and a diameter of ~45–50 μm was loaded into the sample chamber having a thickness 25 μm and diameter of 90 μm in a DAC, together with micro-sized Au powder as the pressure calibrant (Fei et al. 2007b). Neon was also loaded into the sample chamber using the same aforementioned loading procedures. High-pressure X-ray diffraction experiments were conducted at the 13IDD beamline of the GSECARS of the Advanced Photon Source (APS), Argonne National Laboratory (ANL). A monochromatic X-ray beam with a wavelength of 0.3344 Å was focused down to ~5 μm in diameter at the sample position, whereas the diffraction patterns were collected by a MAR CCD. Diffraction patterns were integrated using Fit2D software, and pressures and pressure uncertainties were calculated from the Au pressure calibrant using a third-order Birch-Murnaghan equation of state (BM EoS) and standard error propagation analyses (Birch 1978; Fei et al. 2007b).

RESULTS AND DATA ANALYSES

Raman spectra of the sample were measured in 1–3 GPa intervals up to 73 GPa at ambient temperature (Fig. 1). Four Raman bands were observed and have been identified as translational (T), librational (L), in-plane bend ($ν_4$), and symmetric stretch ($ν_1$) modes from magnesian siderite according to previous studies (e.g., Rutt and Nicola 1974; White 1974; Edwards et al. 2005; Gunasekaran et al. 2006; Rividi et al. 2010; Clark et al. 2011; Santillan et al. 2005; Kaabar et al. 2011) (Figs. 1 and 2), discussed further in the Discussion section. Two other Raman active modes, the anti-symmetric stretch ($ν_3$) and out-of-plane bend ($2ν_2$), were reported previously (Rividi et al. 2010) but were not observed in this study due to the diamond windows. Measured Raman spectra were analyzed using Origin Pro 8 commercial software, in which the Raman bands were fit with a Lorentzian function

(Figs. 1 and 3). The Raman shifts of the modes increased almost linearly with increasing pressure, but changed dramatically at 45 GPa. The transition pressure is consistent with the previously observed spin transition in ferromagnesite (Mattila et al. 2007; Shi et al. 2008; Lavina et al. 2009, 2010a, 2010b; Nagai et al. 2010). All modes increased in Raman shift at 45 GPa except for the internal symmetric mode, which experienced a decrease across the transition (Fig. 3; Table 1). These Raman bands were

clearly split into two bands within the transition, suggesting the presence of two species of differing unit-cell volume, corresponding to either the HS or LS domain; this splitting feature was most prominent in the symmetric mode, which also displayed a satellite peak (v_1') at a slightly higher Raman shift after the transition (Fig. 1). Raman shifts of each mode as a function of pressure can be well modeled by a linear fit before and after the transition, respectively (Fig. 3; Table 1). Once the spin transition has taken place, the changes in Raman shift are again linear functions of increasing pressure in the lower-spin state, although the slopes significantly decrease by as much as 50% (Table 1).

X-ray diffraction patterns were collected from the sample in 1–3 GPa intervals up to 80 GPa at 300 K (Fig. 4). The magnesian siderite unit-cell parameters drop significantly at 45 GPa, consistent with previous studies on the spin transition (Mattila et al. 2007; Lavina et al. 2009, 2010a, 2010b; Nagai et al. 2010) (Figs. 5 and 6). The pressure-volume relation in the high-spin
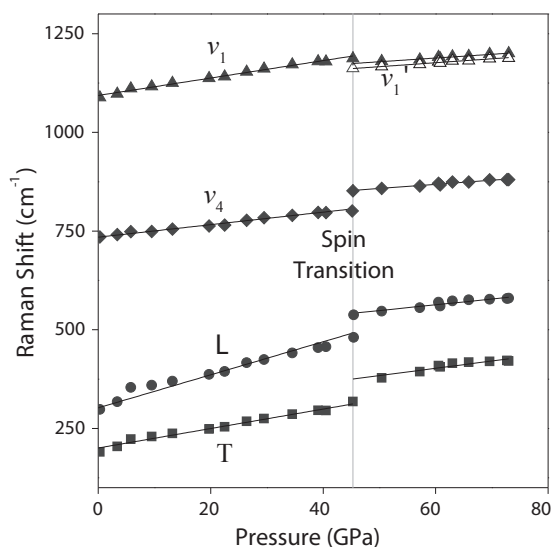

FIGURE 1. Representative Raman spectra of magnesian siderite $(Mg_{0.33}Fe_{0.65})CO_3$ at high pressures. The Raman modes are labeled according to the nomenclatures used in the literature (e.g., Rividi et al. 2010). T = translational lattice mode; L = librational lattice mode; v_1 = symmetric stretching internal mode; v_4 = in-plane bending internal mode. The spin transition of Fe^{2+} at 45 GPa causes significant changes in the spectral features (see Fig. 2). The changes are most evident in the strongest symmetric stretching internal mode (v_1), which is split within the transition and exhibits a satellite band (v_1') after the transition. The broad band at ~500–600 cm^{-1} may be associated with the vibration of a Fe-O band (Buzgar and Apopei 2009). F denotes fluorescence background from sample and diamonds.

FIGURE 3. Raman shifts of magnesian siderite $(Mg_{0.35}Fe_{0.65})CO_3$ at high pressures. The spin transition of Fe^{2+} in the sample at 45 GPa causes significant increases in the Raman shifts of the T, L, and v_4 modes, whereas the Raman shift of the symmetric stretching internal mode (v_1) decreases across the transition. The effects of the spin transition and pressure on the shifts are tabulated in Table 1. Error bars are typically smaller than symbols and are not shown.
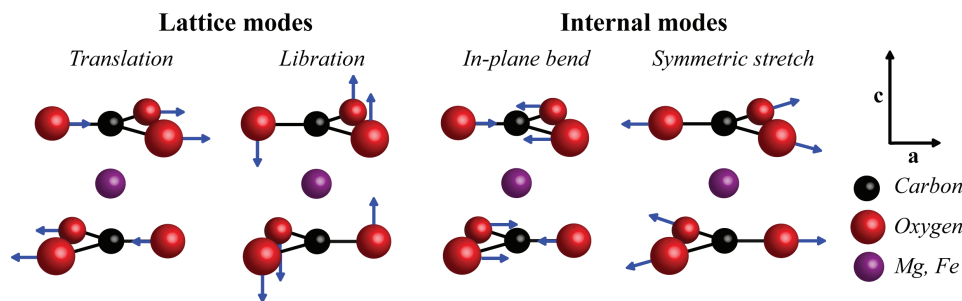

FIGURE 2. Modeled vibrational modes T, L, v_4, and v_1 (same order left to right in figure) observed via Raman spectroscopy from magnesian siderite (after Rividi et al. 2010). Atomic radii are approximately to scale. However, bond lengths as well as c/a axis ratio has been modified to fit the space given. Representative unit-cell structure relative to these modes is found in Figure 5. (Color online.)

TABLE 1. Modeled vibrational parameters of magnesian siderite $(Mg_{0.35}Fe_{0.65})CO_3$ at high pressures

Raman mode		dv/dP (cm⁻¹/GPa)	Raman shift vs. P	Δv (cm⁻¹)	Mode Grüneisen parameter (γ_i)	Mg effect on Raman shift	Δv_o (cm⁻¹)
T	HS	2.51 (±0.10)	ν = 2.51·P + 200	62 (±10)	1.96 (±0.03)	ν = 0.26·Mg no. + 186.6	26 (±3)
	LS	1.86 (±0.16)	ν = 1.86·P + 291		1.69 (±0.03)		
L	HS	3.64 (±0.18)	ν = 3.64·P + 315	58 (±16)	1.87 (±0.03)	ν = 0.40·Mg no. + 289.4	40 (±4)
	LS	1.64 (±0.17)	ν = 1.64·P + 464		1.08 (±0.02)		
ν₄	HS	1.49 (±0.06)	ν = 1.49·P + 735	50 (±7)	0.41 (±0.01)	ν = 0.06·Mg no. + 733.7	6 (±1)
	LS	1.07 (±0.08)	ν = 1.07·P + 804		0.44 (±0.01)		
ν₁	HS	2.17 (±0.07)	ν = 2.17·P + 1093	−17 (±7)	0.39 (±0.01)	ν = 0.08·Mg no. + 1087.3	8 (±1)
	LS (ν₁)	0.94 (±0.09)	ν = 0.94·P + 1132		0.30 (±0.01)		
	LS (ν₁')	1.01 (±0.06)	ν = 1.01·P + 1116		0.31 (±0.01)	–	–

Notes: HS = high-spin state; LS = low-spin state; dv/dP = pressure derivative of the Raman shift. Δv represents the difference of the Raman shifts between the low-spin and high-spin state at 45 GPa. Raman shift difference (Δv_o) between $MgCO_3$ and $FeCO_3$ systems under ambient conditions are also listed for comparison (after Rividi et al. 2010). Mg no. = [100·Mg/(Mg+Fe)] is the ratio of Mg in the solid solution system in percentage. The error bars represent one standard deviation in experimental uncertainties in our study.

and low-spin states, respectively, has been fitted to the Birch-Murnaghan EoS (Birch 1978) to derive the bulk modulus at ambient pressure (K_0) and its pressure derivative (K_0')

$$ P = \frac{3K_0}{2}\left[\left(\frac{V_0}{V}\right)^{\frac{7}{3}} - \left(\frac{V_0}{V}\right)^{\frac{5}{3}}\right]\left\{\left[1 - \frac{3}{4}\left(4 - K_0'\right)\left[\left(\frac{V_0}{V}\right)^{\frac{2}{3}} - 1\right]\right]\right\} $$

where P is pressure, V is the unit-cell volume, and 0 denotes ambient conditions (Fig. 7; Table 2). The bulk modulus, at a given pressure, (K) is calculated from the derived K_0 and K_0', using the BM EoS. Linear incompressibility of each spin state along each unit-cell axis, a or c, is derived from fitting the data to an extended Birch-Murnaghan EoS (Meade and Jeanloz 1990; Liu et al. 2003) (Fig. 6; Table 2), in which the Eulerian finite strain (f) is expressed as

$$ f_a = \frac{1}{2}\left[\left(\frac{a_0}{a}\right)^2 - 1\right] $$

and

$$ f_c = \frac{1}{2}\left[\left(\frac{c_0}{c}\right)^2 - 1\right] $$

respectively.

Discussion

Lattice vibration across the spin transition

The measured Raman shifts of magnesian siderite $[(Mg_{0.35}Fe_{0.65})CO_3]$ at ambient conditions lie between two end-members, magnesite and siderite (Table 1). The rhombohedral magnesian siderite unit cell consists of $(CO_3)^{2-}$ anions and divalent cations (Mg^{2+} and Fe^{2+}), similar to the end-member carbonates. Because Fe^{2+} randomly substitutes for Mg^{2+} in magnesian siderite, there is no loss of rotational symmetry (Bischoff et al. 1985). Via factor group analysis, members of a solid solution are predicted to have Raman spectra similar to those of the end-members but with a continuous shift in wavenumbers (White 1974). Previous studies on Raman shifts of carbonates have attributed low-wavenumber bands to lattice vibrational modes and high-wavenumber bands to internal vibrational modes (e.g., Rutt and Nicola 1974; White 1974; Edwards et al. 2005; Gunasekaran et al. 2006; Rividi et al. 2010; Clark et al. 2011; Kaabar et al.
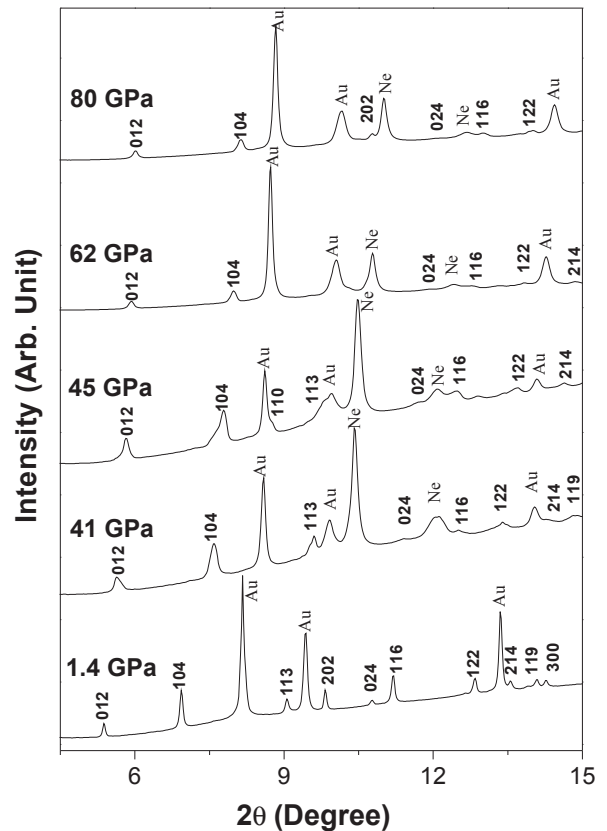

FIGURE 4. Representative angle-dispersive X-ray diffraction spectra of magnesian siderite $(Mg_{0.35}Fe_{0.65})CO_3$ at high pressures. Gold power (Au) was used as the pressure calibrant (Fei et al. 2007b), whereas neon (Ne) was used as the pressure medium. The occurrence of the spin transition of Fe^{2+} in the sample at 45 GPa causes the diffraction peaks to split between the high-spin and low-spin states, indicating two distinct volumes. Incident X-ray wavelength λ = 0.3344 Å.

2011). Based on these results, the lower-frequency, lower-intensity band at 190 cm⁻¹ was assigned to the translational mode (T) and the high-frequency, higher-intensity band at 298 cm⁻¹ to the librational mode (L) (Figs. 1–2; Table 1). The internal vibrational symmetric stretch mode ($ν_1$) produces the most intense Raman band at 1088 cm⁻¹, whereas another internal first-order band at 734 cm⁻¹ corresponds to the in-plane bend (or symmetric bend) mode ($ν_4$) (White 1974) (Figs. 1–2; Table 1).
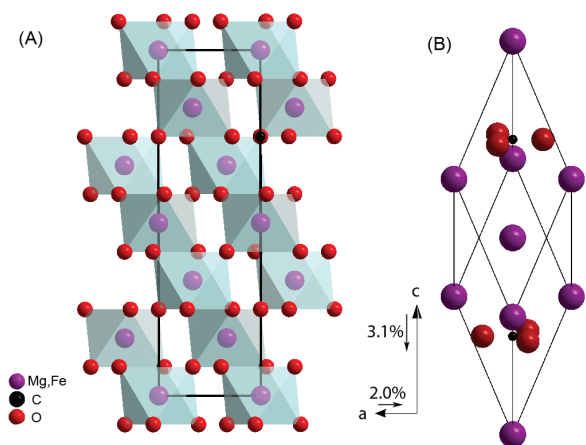
FIGURE 5. (**a**) Visual representation of the unit cell of magnesian siderite. The percentage of volume collapse after the spin transition at 45 GPa is also shown for *c* and *a* axes. Unit parameters are based on our results at 45 GPa; atom positions are taken from Lavina et al. (2010a, 2010b). (**b**) Rhombohedral representation of the crystal structure of magnesian siderite. The motions of the $(CO_3)^{2-}$ units relative to the central cation that result in the observed vibrational modes can be found in Figure 2. (Color online.)

FIGURE 6. Lattice parameters of magnesian siderite $(Mg_{0.35}Fe_{0.65})CO_3$ at high pressures. Ratios of the unit-cell constants, *a* and *c*, as a function of pressure. Dashed lines represent BM EoS fits to the data. The spin transition of Fe^{2+} in the sample at 45 GPa causes these cell parameters to decrease significantly. Uncertainties are smaller than symbols when not shown. c/c_0 and a/a_0 values are shown in the left vertical axis, whereas c/a values are shown in the right vertical axis.

Replacing the sixfold-coordinated Mg^{2+} (ionic radius = 0.68 Å) with the larger Fe^{2+} (high-spin ionic radius = 0.74 Å) (Shannon and Prewitt 1969), at ambient conditions, increases the interatomic distances between the (Mg^{2+}, Fe^{2+}) cation and the $(CO_3)^{2-}$ anion in the unit cell of ferromagnesite, decreasing the vibrational frequency (e.g., Rutt and Nicola 1974; White 1974). This has been shown to account for most, if not all, of the range of Raman shifts in the $MgCO_3$-$FeCO_3$ solid solutions (Rividi et al. 2010) (Tables 1–2). Indeed, the Raman shift values for the lattice modes show displacement to higher values following the increase of magnesium content in ferromagnesite (Table 1). This compositional effect is most prominent in the external lattice modes (*T* and *L*), but much less evident in the internal modes (ν_1 and ν_4), as the covalent C-O bonds of the rhombohedral $(CO_3)^{2-}$ group are poorly sensitive to cation substitutions (White 1974).

In combination with the X-ray diffraction results, the sharp Raman shift increase in the *T, L,* and ν_4 modes and subtle drop in ν_1 modes at 45 GPa can be well explained as a result of the spin transition. The transition causes a decrease in volume and in octahedral bond distance, an increase in bulk modulus, and a slight increase in the C-O bond length of the $(CO_3)^{2-}$ units (Lavina et al. 2009, 2010a, 2010b; Nagai et al. 2010). That is, the low-spin state exhibits a stiffer unit-cell lattice and smaller bond distances between neighboring $(CO_3)^{2-}$ units than the end-member magnesite (Figs. 5–7) (Lavina et al. 2009, 2010a, 2010b; Nagai et al. 2010). At ambient conditions, high-spin Fe^{2+} substitution increases the unit-cell size of magnesite, causing a vibrational frequency decrease. However, low-spin Fe^{2+} is a smaller cation than Mg^{2+}, decreasing the unit-cell volume to smaller than that of magnesite as well as high-spin magnesian siderite, thereby contributing to an increase in Raman shift over the transition (Lavina et al. 2009) (Fig. 7). For the high-spin state, structural refinements on single-crystal magnesian siderite also showed that over 45 GPa, the strong C-O bond initially decreases in
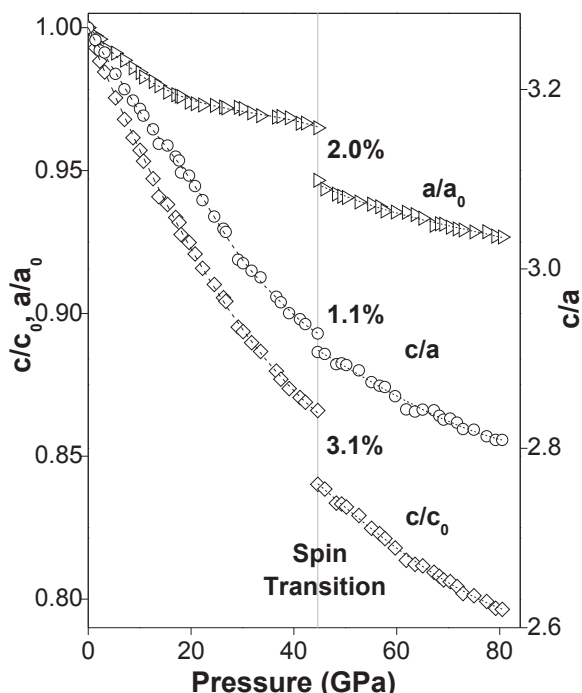
length by only 2–3% (0.03 Å), but experiences an appreciable lengthening with pressure increase after the transition (Lavina et al. 2010a). Therefore, there are two competing factors present: the unit-cell stiffness and bulk modulus increases, and volume decrease, contribute to vibrational frequency increases; the C-O bond lengthening along the *a* axis and within the planar $(CO_3)^{2-}$ unit facilitates a vibrational frequency decrease. The lattice modes (*T, L*) are strongly coupled to the lattice volume and are prominently affected by the volume collapse, showing increases in Raman shift over the transition. The internal modes (ν_4, ν_1) are more susceptible to the C-O bond lengthening; however, only the symmetric stretch experiences a decrease in Raman shift, showing that the bond lengthening effect wins over the lattice contraction effect. The lattice contraction effect overcompensates for the frequency decreasing effects of the bond lengthening, effectively increasing the Raman shift of the in-plane bend. The small, broad satellite peak (ν_1') could be assigned to the effect of increased proximity (and thus magnitude of the electronic interaction) between neighboring $(CO_3)^{2-}$ units in the low-spin state, leading to a range of Raman frequencies (see ν_1 peak broadening after the transition in Fig. 1) caused by in-phase and out-of-phase vibrations of adjacent $(CO_3)^{2-}$ units.

Lattice parameters and equation of state

Analyses of the compression data using the BM EoS show that the high-pressure, low-spin state exhibits a higher modulus

TABLE 2. Equation of state parameters of ferromagnesite at high pressures

	$(Fe_{0.65}Mg_{0.33}Mn_{0.02})CO_3$ This study		$(Fe_{0.72}Mg_{0.24}Mn_{0.03}Ca_{0.01})CO_3$ Lavina et al. (2009, 2010a)		$(Fe_{0.12}Mg_{0.87}Ca_{0.01})CO_3$ Lavina et al. (2010b)		$(Fe_{0.73}Mg_{0.22}Mn_{0.05})CO_3$ Nagai et al. (2010)	
	HS	LS	HS	LS	HS	LS	HS	LS
V_0 (Å³)	289.1(±0.1)	267(±2)	294.4(±0.3)	263(±3)	281.0(±0.5)	–	293.5(±0.1)	–
K_0 (GPa)	108(±2)	127(±5)	110.1(±0.8)	148(±12)	102.8(±0.3)	–	120(±3)	–
K_0'	4.8(±0.2)	5.1(±0.2)	4.6(±0.2)	5	5.44	–	4.3(±0.3)	–
a (Å)	4.487 (±0.001)	4.419 (±0.004)	4.480 (±0.008)	4.420 (±0.003)	4.369 (±0.006)	4.349 (±0.006)	4.500 (±0.004)	4.396 (±0.03)
c (Å)	13.15 (±0.02)	12.84 (±0.02)	13.60 (±0.01)	13.01 (±0.04)	13.27 (±0.05)	13.16 (±0.054)	13.22 (±0.06)	12.83 (±0.02)
$\Delta V/V$ (%)	8.1(±0.3)		10.4		–		6.5	

Notes: The parameters are modeled using the third-order Birch-Murnaghan EoS (Birch 1978). a and c represent the cell parameters calculated from the X-ray diffraction patterns right before and after the spin transition at 45 GPa. $\Delta V/V$ is the percentage of the volume decrease across the spin transition. The error bars represent one standard deviation in experimental uncertainties in our study.

than the low-pressure, high-spin state; the bulk modulus jumps by ~9.8% across the transition in $(Mg_{0.35}Fe_{0.65})CO_3$ (Figs. 8 and 9). Such effects of the spin transition on incompressibility have also been reported to occur in lower-mantle ferropericlase (e.g., Lin et al. 2005, 2009; Speziale et al. 2007; Marquardt et al. 2009; Komabayashi et al. 2010). High-spin magnesian siderite displays a similar incompressibility to magnesite before the transition (Fig. 9b), indicating that the addition of iron has negligible effects on incompressibility. The low-spin state of magnesian siderite is ~5–7% stiffer than magnesite at similar conditions (Fiquet et al. 2002) (Fig. 9). The unit-cell volume of high-spin magnesian siderite is ~4% higher than that of magnesite, but drops by 5.7% at the spin transition (Fig. 5); that is, low-spin magnesian siderite is ~2% smaller in unit-cell volume than magnesite (Fig. 9). The smaller-volume, low-spin ferromagnesite has been suggested to increase in stability in the lower mantle, and could therefore become a candidate accessory mineral for deep-carbon storage (Lavina et al. 2009). However, ferromagnesite has been recently shown to transform into an assemblage of compounds at lower-mantle conditions (Boulard et al. 2011). Thus, it is yet to be understood how the spin transition affects the phase diagram of ferromagnesite at relevant conditions of the lower mantle.

The c and a axes show strong anisotropic compression with the c axis being much more compressible than the a axis. Across the spin transition, the length of the c axis decreases by 3.1%, the a axis by 2.0%, and the c/a ratio by 1.1% (Figs. 5 and 6). The axial linear incompressibility parameters along each one of the two unit-cell axes, a or c, are fitted with the extended Eulerian finite-strain EoS using the third-order BM EoS (Birch 1978; Liu et al. 2003). For the a axis, the high-spin state has $K_0 = 210$ (±7) GPa with $K_0' = 8.2$ (±0.5), whereas the low-spin state has $K_0 = 212$ (±9) GPa with $K_0' = 8.6$ (±0.7). For the c axis, the high-spin state has $K_0 = 64.1$ (±0.7) GPa with $K_0' = 2.52$ (±0.03) and the low-spin state has $K_0 = 50.6$ (±1.4) GPa with $K_0' = 3.49$ (±0.08).

Structurally, the planar $(CO_3)^{2-}$ units are oriented perpendicular to the c axis and the individual C-O bonds are aligned parallel to the a axis (Fig. 5). The large anisotropy of compression suggests that the rigid $(CO_3)^{2-}$ units contribute to the highly incompressible behavior along the a axis through strong, covalent C-O bonds and oxygen repulsion (Lavina et al. 2010b). As discussed earlier, space group $R\bar{3}c$ of carbonates can be described as a distortion of the NaCl structure along [111] direction. A convenient parameter describing the degree of distortion from the NaCl structure is defined as $t = 4a/\sqrt{2}\,c$, a ratio between the a and c axes (e.g., Wells 1984; Fiquet et al. 1994). Whereas most carbonates have t values between 0.8 and 0.9, this distortion parameter is equal to
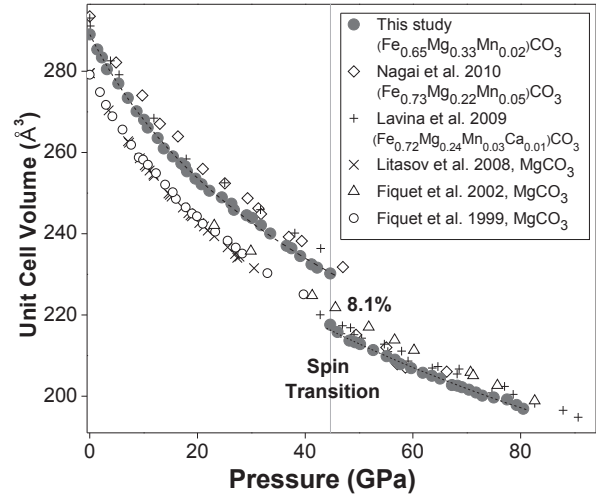

FIGURE 7. Comparison of the pressure-volume relations in the $(Mg,Fe)CO_3$ system (Fiquet and Reynard 1999; Litasov et al. 2008; Lavina et al. 2009, 2010a; Nagai et al. 2010). The volume collapse across the spin transition is 8.1% in our $(Mg_{0.35}Fe_{0.65})CO_3$ sample. Dashed lines represent BM EoS fits to the data.

one in an ideal NaCl structure (Fiquet et al. 1994). Evaluation of the parameter as a function of pressure shows that our magnesian siderite has $t = 0.86$, similar to that of magnesite at ambient conditions (Fiquet et al. 1994). The parameter increases significantly with increasing pressure and approaches 0.97 at the spin transition pressure of 45 GPa where the slope decreases significantly. That is, the spin transition also affects the distortion parameter of the magnesian siderite at high pressures. The parameter is almost equal to 1 at ~72 GPa (Lavina et al. 2009, 2010a; Nagai et al. 2010) (Fig. 10). We note that magnesite has a smaller t of 0.96 at the same pressure (Fiquet et al. 2002). Thus, this suggests that the arrangement of the Fe^{2+} and $(CO_3)^{2-}$ ions in the low-spin magnesian siderite at 70–80 GPa is very similar to the ideal NaCl structure. Since the c axis is much more compressible than the a axis, the distortion parameter eventually is larger than one. This indicates that the low-spin magnesian siderite lattice can be described as a distortion of the NaCl structure being compressed along [111] direction at pressures above ~72 GPa, instead being elongated along the direction at lower pressures.

Mode Grüneisen parameter

The combined Raman and X-ray diffraction results are used to derive the mode Grüneisen parameter (γ), an important ther-
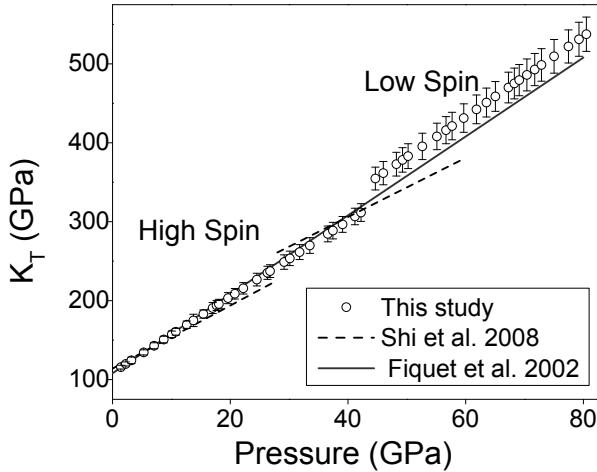
FIGURE 8. Isothermal bulk modulus (K_T) of magnesian siderite ($Mg_{0.35}Fe_{0.65}$)CO_3 compared to that of magnesite at high pressures. The solid line represents calculated K_T of magnesite using K_{0T} = 108 GPa and K_0' = 5 (Fiquet et al. 2002). Dashed lines represent theoretical calculations on siderite by Shi et al. (2008). The K_T of magnesian siderite from this study increases by ~10% across the spin transition at 45 GPa. These values and their errors are calculated based on the BM EoS. Error bars span two standard deviations.
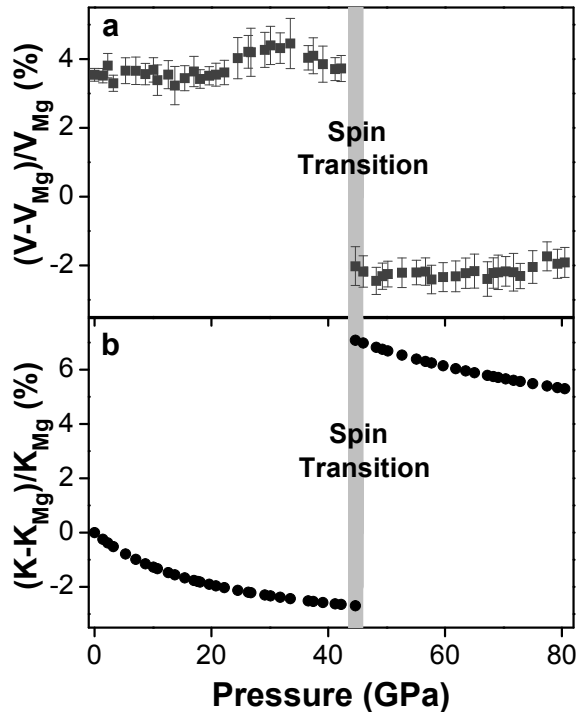
modynamic parameter for characterizing the high P-T behavior of planetary materials (Anderson 2000). The measured vibrational frequency (v), as a function of pressure (P) or volume (V), represents a mode Grüneisen parameter for the phonon mode following the equation (Born and Huang 1954)

$$\gamma_i = \frac{d\ln v_i}{d\ln V} = \frac{K_T}{v_i}\left(\frac{dv_i}{dP}\right).$$

This parameter links variation in vibrational frequency to changes in crystal lattice volume and, as a consequence, to the effect of changing temperature on the size or dynamics of the lattice (Wagner 2000). The parameter thus reflects not only the differing mass and ionic radius of substituting cations in magnesian siderite, but also the compression of the carbonate ion. The mode Grüneisen parameters for magnesian siderite were calculated using the linear fits to the Raman data and the derived EoS parameters from the pressure-volume relationship (Table 1). The mode Grüneisen parameters of the high-spin state for the two external lattice modes (T and L) are 1.96 and 1.87, respectively, but these values drop to 1.69 and 1.08 in the low-spin state. On the other hand, the mode Grüneisen parameters of the two internal modes (v_1 and v_4) are much less affected by the spin transition (Table 1). These suggest that the low-spin state has distinctive vibrational and elastic properties from that of the high-spin state (e.g., Shi et al. 2008; Wentzcovitch et al. 2009). To calculate the average of the mode Grüneisen parameters ($\bar{\gamma}$) meaningfully, one has to weight each mode by the heat capacity for that mode, but such information is unavailable for the low-spin state. The average thermodynamic Grüneisen parameter (γ_{th}),

FIGURE 9. Comparison of unit-cell volume (**a**) and isothermal bulk modulus (**b**) between magnesian siderite ($Mg_{0.35}Fe_{0.65}$)CO_3 and magnesite. V_{Mg} and K_{Mg} are the unit-cell volume (V) and the isothermal bulk modulus (K) of magnesite calculated using the EoS parameters given by Fiquet et al. (2002) (V_0 = 279.2 Å^3, K_{0T} = 108 GPa, and K_0' = 5). Error bars span two standard deviations. The errors are smaller than the symbol in **b**.
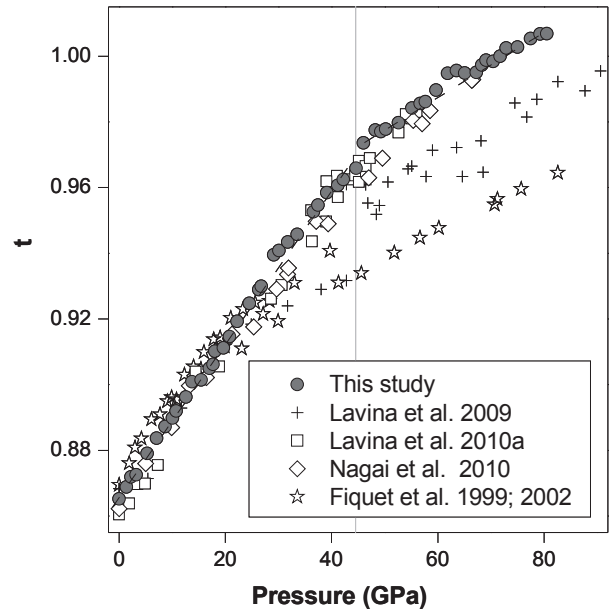

FIGURE 10. Distortion parameter ($t = 4a/\sqrt{2}c$) as a function of pressure. This parameter is used to describe the degree of distortion in rhombohedral carbonates from the NaCl structure. The vertical, solid gray area represents the pressure range of the spin transition zone. Previous studies on magnesite (Fiquet and Reynard 1999; Fiquet et al. 2002) and magnesian siderite (Lavina et al. 2009, 2010a; Nagai et al. 2010) are also plotted for comparison. Dashed lines represent BM EoS fits to the data.
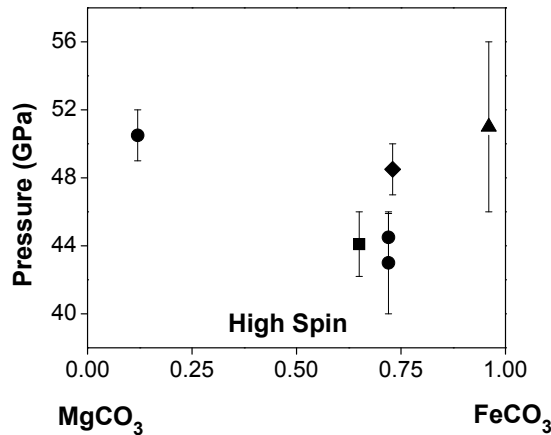
FIGURE 11. Spin transition pressure in correlation to the magnesite-siderite solid-solution system under high pressures at room temperature. Solid square = X-ray diffraction and Raman spectroscopy (this study); solid circles = X-ray diffraction (Lavina et al. 2009, 2010a, 2010b); solid diamond = X-ray diffraction (Nagai et al. 2010); solid triangle = X-ray emission (Mattila et al. 2007). The error bars span two standard deviations in experimental uncertainties in our study and the literature.

which takes all contributions of the parameter into account, can also be calculated using the following thermodynamic relation

$$\gamma_{th} = \frac{\alpha K_S}{\rho C_P} = \frac{\alpha K_T}{\rho C_V}$$

where ρ is the density, K_S and K_T are the adiabatic and isothermal bulk modulus, respectively, and C_P and C_V are the heat capacity at constant pressure and volume, respectively. Using values of $\alpha = 2.98 \times 10^{-5}$ K^{-1} (Zhang et al. 1998), $\rho = 3656$ kg/m^3 (this study), $K_S = 109$ GPa (estimated from this study), and $C_P = 81.3$ J/(mol·K) (Robie et al. 1984) at 300 K, the thermodynamic Grüneisen parameter of the high-spin state is ~1.1. The low-spin state is expected to have a lower thermodynamic Grüneisen parameter, but data on its thermal expansion coefficient and heat capacity are still unavailable.

Pressure-composition correlation

To understand the compositional effect on the spin transition in the system, we have plotted all literature transition pressures as a function of composition (Mattila et al. 2007; Lavina et al. 2009, 2010a, 2010b; Nagai et al. 2010) (Fig. 11). Even though these studies were carried out under various experimental conditions using different techniques, the transition pressures fall on a narrow range between 42 and 50 GPa for almost all of the compositional range. The negligible compositional effect on the transition pressure in the (Mg,Fe)CO$_3$ system can be explained by much longer Fe^{2+}-Fe^{2+} distances in the structure, separated by the (CO$_3$)$^{2-}$ units (Fig. 5). Although the system can contain up to 20 at% of Fe^{2+} in the end-member FeCO$_3$, the Fe^{2+}-Fe^{2+} exchange interactions between distant neighboring Fe^{2+} atoms are below the percolation threshold and have a negligible effect on the transition pressure. This is unlike the spin transition in ferropericlase, in which the contribution of the Fe^{2+}-Fe^{2+} exchange interactions in FeO-rich part is known to stabilize the high-spin state to much higher pressures (Lin et al. 2006).

REFERENCES CITED

Anderson, O.L. (2000) The Grüneisen ratio for the last 30 years. Geophysical Journal International, 143, 279–294.
Biellmann, C., Gillet, P., Guyot, F., Peyronneau, J., and Reynard, B. (1993) Experimental evidence for carbonate stability in the Earth's lower mantle. Earth and Planetary Science Letters, 118, 31–41.
Birch, F. (1978) Finite strain isotherm and velocities for single crystal and polycrystalline NaCl at high pressure and 300 K. Journal of Geophysical Research, 83, 1257–1268.
Bischoff, W.D., Sharma, S.K., and Mackenzie, F.T. (1985) Carbonate ion disorder in synthetic and biogenic magnesian calcites: A Raman spectral study. American Mineralogist, 70, 581–589.
Born, M. and Huang, K. (1954) Dynamical theory of crystal lattices. Oxford University Press, U.K.
Boulard, E., Gloter, A., Corgne, A., Antonangeli, D., Auzende, A.L., Perrillat, J.P., Guyot, F., and Fiquet, G. (2011) New host for carbon in the deep Earth. Proceedings of the National Academy of Sciences, 108, 5184–5187.
Brenker, F.E., Vollmer, C., Vincze, L., Vekemans, B., Szymanski, A., Janssens, K., Szaloki, I., Nasdala, L., Joswig, W., and Kaminsky, F. (2007) Carbonates from the lower part of transition zone or even the lower mantle. Earth and Planetary Science Letters, 260, 1–9.
Buzgar, N. and Apopei, A. (2009) The Raman study of certain carbonates. Geologie. Tomul LV, 2, 97–112.
Clark, S.J., Jouanna, P., Haines, J., and Mainprice, D. (2011) Calculation of infrared and Raman vibration modes of magnesite at high pressure by density-functional perturbation theory and comparison with experiments. Physics and Chemistry of Minerals, 38, 193–202.
Crowhurst, J.C., Brown, J.M., Goncharov, A.F., and Jacobsen, S.D. (2008) Elasticity of (Mg,Fe)O through the spin transition of iron in the lower mantle. Science, 319, 451–453.
Dasgupta, R. and Hirschmann, M.M. (2010) The deep carbon cycle and melting in Earth's interior. Earth and Planetary Science Letters, 298, 1–13.
Edwards, H.G.M., Jorge Villar, S.E., Jehlicka, J., and Munshi, T. (2005) FT-Raman spectroscopic study of calcium-rich and magnesium-rich carbonate minerals. Spectrochimica Acta Part A, 61, 2273–2280.
Fei, Y., Zhang, L., Corgne, A., Watson, H., Ricolleau, Meng, Y., and Prakapenka, V. (2007a) Spin transition and equations of state of (Mg,Fe)O solid solutions. Geophysical Research Letters, 34, L17307.
Fei, Y., Ricolleau, A., Frank, M., Mibe, K., Shen, G., and Prakapenka, V. (2007b) Towards an internally consistent pressure scale. Proceedings of the National Academy of Sciences, 104, 9182–9186.
Fiquet, G. and Reynard, B. (1999) High-pressure equation of state of magnesite: new data and a reappraisal. American Mineralogist, 84, 856–860.
Fiquet, G., Guyot, F., and Itie, J.P. (1994) High-pressure X-ray diffraction study of carbonates: MgCO$_3$, CaMg(CO$_3$)$_2$, and CaCO$_3$. American Mineralogist, 79, 15–23.
Fiquet, G., Guyot, F., Kunz, M., Matas, J., Andrault, D., and Hanfland, M. (2002) Structural refinements of magnesite at very high pressure. American Mineralogist, 87, 1261–1265.
Ghosh, S., Ohtani, E., Litasov, K.D., and Terasaki, H. (2009) Solidus of carbonated peridotite from 10 to 20 GPa and origin of magnesiocarbonatite melt in the Earth's deep mantle. Chemical Geology, 262, 17–28.
Gillet, P., Biellmann, C., Reynard, B., and McMillan, P. (1993) Raman spectroscopic studies of carbonates Part I: High-pressure and high-temperature behaviour of calcite, magnesite, dolomite and aragonite. Physics and Chemistry of Minerals, 20, 1–18.
Gunasekaran, S., Anbalagan, G., and Pandi, S. (2006) Raman and infrared spectra of carbonates of calcite structure. Journal of Raman Spectroscopy, 37, 892–899.
Isshiki, M., Irifune, T., Hirose, K., Ono, S., Ohishi, Y., Watanuki, T., Nishibori, E., Takata, M., and Sakata, M. (2004) Stability of magnesite and its high-pressure form in the lowermost mantle. Nature, 427, 60–63.
Javoy, M. (1997) The major volatile elements of the Earth: Their origin, behaviour, and fate. Geophysical Research Letters, 24, 177–180.
Kaabar, W., Botta, S., and Devonshire, R. (2011) Raman spectroscopic study of mixed carbonate materials. Spectrochimica Acta Part A, 78, 136–141.

Katsura, T. and Ito, E. (1990) Melting and subsolidus phase-relations in the MgSiO$_3$-MgCO$_3$ system at high-pressures: Implications to evolution of the Earth's atmosphere. Earth and Planetary Science Letters, 99, 110–117.

Kaminsky, F.V. and Wirth, R. (2011) Iron carbide inclusions in lower-mantle diamond from Juina, Brazil. The Canadian Mineralogist, 49, 555–572.

Komabayashi, T., Hirose, K., Nagaya, Y., Sugimura, E., and Ohishi, Y. (2010) High temperature compression of ferropericlase and the effect of temperature on iron spin transition. Earth and Planetary Science Letters, 297, 691–699.

Lavina, B., Dera, P., Downs, R.T., Prakapenka, V., Rivers, M., Sutton, S., and Nicol, M. (2009) Siderite at lower mantle conditions and the effects of the pressure-induced spin-pairing transition. Geophysical Research Letters, 36, L23306.

Lavina, B., Dera, P., Downs, R.T., Yang, W., Sinogeikin, S., Meng, Y., Shen, G., and Schiferl, D. (2010a) Structure of siderite FeCO$_3$ to 56 GPa and hysteresis of its spin-pairing transition. Physical Review B, 82, 064110.

Lavina, B., Dera, P., Downs, R.T., Tschauner, O.T., Yang, W., Shebanova, O., and Shen, G. (2010b) Effect of dilution on the spin pairing transition in rhombohedral carbonates. High Pressure Research, 30, 224–229.

Li, L. and Fei, Y. (2003) Experimental constraints on core composition. In R.W. Carlson, Ed., The Mantle and Core, 2nd edition, Volume 2, p. 521–546. Treatise on Geochemistry, Elsevier, Amsterdam.

Lin, J.F., Struzhkin, V., Jacobsen, S.D., Hu, M., Chow, P., Kung, J., Liu, H., Mao, H.K., and Hemley, R.J. (2005) Spin transition of iron in magnesiowüstite in Earth's lower mantle. Nature, 436, 377–380.

Lin, J.F., Gavriliuk, A.G., Struzhkin, V.V., Jacobsen, S.D., Sturhahn, W., Hu, M.Y., Chow, P., and Yoo, C.S. (2006) Pressure-induced electronic spin transition of iron in magnesiowüstite-(Mg,Fe)O. Physical Review B, 73, 113107.

Lin, J.F., Weir, S.T., Jackson, D.D., Evans, W.J., and Yoo, C.S. (2007) Electrical conductivity of the low-spin ferropericlase in the Earth's lower mantle. Geophysical Research Letters, 34, L16305, 2007.

Lin, J.F. and Tsuchiya, T. (2008) Spin transition of iron in the Earth's lower mantle. Physics of the Earth and Planetary Interiors, 170, 248–259.

Lin, J.F., Wenk, H.R., Voltolini, M., Speziale, S., Shu, J., and Duffy, T.S. (2009) Deformation of lower-mantle ferropericlase (Mg,Fe)O across the electric spin transition. Physics and Chemistry of Minerals, 36, 585–592.

Litasov, K.D., Fei, Y., Ohtani, E., Kuribayashi, T., and Funakoshi, K. (2008) Thermal equation of state of magnesite to 32 GPa and 2073 K. Physics of the Earth and Planetary Interiors, 168, 191–203.

Liu, H., Caldwell, W.A., Benedetti, L.R., Panero, W., and Jeanloz, R. (2003) Static compression of α-Fe$_2$O$_3$: linear incompressibility of lattice parameters and high-pressure transformations. Physics and Chemistry of Minerals, 30, 582–588.

Mao, H.K., Bell, P.M., Shaner, J.W., and Steinberg, D.J. (1978) Specific volume measurements of Cu, Mo, Pd, and Ag and calibration of the ruby R_1 fluorescence pressure gauge from 0.06 to 1 Mbar. Journal of Applied Physics, 49, 3276–3283.

Marquardt, H., Speziale, S., Reichmann, H.J., Frost, D.J., Schilling, F.R., and Garnero, E.J. (2009) Elastic shear anisotropy of ferropericlase in Earth's lower mantle. Science, 324, 224–226.

Mattila, A., Pylkkänen, T., Rueff, J.P., Huotari, S., Vanko, G., Hanfland, M., Lehtinen, M., and Hämäläinen, K. (2007) Pressure induced magnetic transition in siderite FeCO$_3$ studied by X-ray emission spectroscopy. Journal of Physics: Condensed Matter, 19, 386206.

McDonough, W.F. and Sun, S.-s. (1995) The composition of the Earth. Chemical Geology, 120, 223–253.

Meade, C. and Jeanloz, R. (1990) Static compression of Ca(OH)$_2$ at room temperature: Observations of amorphization and equation of state measurements to 10.7 GPa. Geophysical Research Letters, 17, 1157–1160.

Nagai, T., Ishido, T., Seto, Y., Nishio-Hamane, D., Sata, N., and Fujino, K. (2010) Pressure-induced spin transition in FeCO$_3$-siderite studied by X-ray diffraction measurements. Journal of Physics: Conference Series, 215, 012002.

Oganov, A.R., Ono, S., Ma, Y., Glass, C.W., and Garcia, A. (2008) Novel high-pressure structures of MgCO$_3$, CaCO$_3$, and CO$_2$ and their role in Earth's lower mantle. Earth and Planetary Science Letters, 273, 38–47.

Pal'yanov, Y.N., Sokol, A.G., Borzdov, Y.M., Khokhryakov, A.F., and Sobolev, N.V. (1999) Diamond formation from mantle carbonate fluids. Nature, 400, 417–418.

Rividi, N., van Zuilen, M., Philippot, P., Menez, B., Godard, G., and Poidatz, E. (2010) Calibration of carbonate composition using micro-Raman analysis: application to planetary surface exploration. Astrobiology, 10, 293–309.

Robie, R.A., Haselton, H.T. Jr., and Hemingway, B.S. (1984) Heat capacities and entropies of rhodochrosite (MnCO$_3$) and siderite (FeCO$_3$) between 5 and 600 K. American Mineralogist, 69, 349–357.

Rohrbach, A. and Schmidt, M.W. (2011) Redox freezing and melting in the Earth's deep mantle resulting from carbon–iron redox coupling. Nature, 472, 209–212.

Rutt, H.N. and Nicola, J.H. (1974) Raman spectra of carbonates of calcite structure. Journal of Physics C: Solid State Physics, 7, 4522–4528.

Santillan, J. and Williams, Q. (2004) A high-pressure infrared and X-ray study of FeCO$_3$ and MnCO$_3$: Comparison with CaMg(CO$_3$)$_2$-dolomite. Physics of the Earth and Planetary Interiors, 143-144, 291–304.

Santillan, J., Catalli, K., and Williams, Q. (2005) An infrared study of carbon-oxygen bonding in magnesite to 60 GPa. American Mineralogist, 90, 1669–1673.

Seto, Y., Hamane, D., Nagai, T., and Fujino, K. (2008) Fate of carbonates within oceanic plates subducted to the lower mantle, and a possible mechanism of diamond formation. Physics and Chemistry of Minerals, 35, 223–229.

Shannon, R.D. and Prewitt, C.T. (1969) Effective ionic radii in oxides and fluorides. Acta Crystallography, B25, 925–945.

Shcheka, S., Wiedenbeck, M., Frost, D., and Keppler, H. (2006) Carbon solubility in mantle minerals. Earth and Planetary Science Letters, 245, 730–742.

Shi, H., Luo, W., Johansson, B., and Ahuja, R. (2008) First-principles calculations of the electronic structure and pressure-induced magnetic transition in siderite FeCO$_3$. Physical Review B, 78, 155119.

Speziale, S., Milner, A., Lee, V.E., Clark, S.M., Pasternak, M., and Jeanloz, R. (2005) Iron spin transition in Earth's mantle. Proceedings of the National Academy of Sciences, 102, 17918–17922.

Speziale, S., Lee, V.E., Clark, S.M., Lin, J.F., Pasternak, M.P., and Jeanloz, R. (2007) Effects of Fe spin transition on the elasticity of (Mg,Fe)O magnesiowüstites and implications for the seismological properties of the Earth's lower mantle. Journal of Geophysical Research, 112, B10212.

Stachel, T., Harris, J.W., Brey, G.P., and Joswig, W. (2000) Kankan diamonds (Guinea) II: Lower mantle inclusion parageneses. Contributions to Mineralogy and Petrology, 140, 16–27.

Stagno, V. and Frost, D.J. (2010) Carbon speciation in the asthenosphere: Experimental measurements of the redox conditions at, which carbonate-bearing melts coexist with graphite or diamond in peridotite assemblages. Earth and Planetary Science Letters, 300, 72–84.

Wagner, J.-M. (2000) On the inadequacy of linear pressure dependence of vibrational frequency. Solid State Communications, 116, 355–356.

Wells, A.F. (1984) Structural Inorganic Chemistry, 5th edition, 1382 p. Clarendon, Oxford, U.K.

Wentzcovitch, R.M., Justo, J.F., Wu, Z., da Silva, C.R.S., Yuen, D.A., and Kohlstedt, D. (2009) Anomalous compressibility of ferropericlase throughout the iron spin cross-over. Proceedings of the National Academy of Sciences, 106, 8447–8452.

White, W.B. (1974) Order-disorder effects. In V.C. Farmer, Ed., Infrared Spectra of Minerals, p. 87–110. Mineralogical Society Monograph 4, London.

Zhang, J., Martinez, I., Guyot, F., and Reeder, R. (1998) Effects of Mg-Fe^{2+} substitution in calcite-structure carbonates: Thermoelastic properties. American Mineralogist, 83, 280–287.